

## THE AFFINE PROJECTION MODEL AS A TOOL FOR RAPID GEO-CODING OF IRS-P5 SATELLITE IMAGERY

F. Dadras Javan<sup>a\*</sup>, A. Azizi<sup>b</sup>

<sup>a</sup>Dept. of Geomatic Engineering, Faculty of Engineering, University of Tehran, Iran - fdadrasjavan@ut.ac.ir

<sup>b</sup>Centre of Excellence for Disaster Management, Dept. of Geomatic Engineering, College of Engineering, University of Tehran, Iran - aazizi@ut.ac.ir

**KEY WORDS:** High Resolution, Pushbroom, IRS-P5, Mapping, Sensor Modeling, Rational Function Model, 3D affine transformation, Hazards

### ABSTRACT:

Nowadays, the information content of the satellite imageries as a means for the disaster forecasting and management has attracted the worldwide attention more than before. On the other hand, linear array satellite images such as Spot, Ikonos, QuickBird, IRS, etc., with their flexibility in acquiring stereo coverage over any part of the globe, have proven to be an excellent replacement for the other space-borne imaging systems such as digital frame cameras or whiskbroom technologies. The first step for using such data is Geo-coding. High resolution data increase the need for higher accuracy data modeling. Up to now different models with different accuracy have been discussed. These models are divided into two main groups of the so called rigorous and non-rigorous models. The rigorous approaches are the most accurate but need crucial data such as satellite ephemeris and inner orientation parameters which are not always available. The non-rigorous models such as rational polynomials, DLT or 3D affine transformations on the other hand are less accurate but enjoy the advantage of being independent from the auxiliary information. In line with several other research works already performed by other researchers, this paper sets its main goal to compare the simple 3D affine model, as a replacement transformation for the more sophisticated rational function approach. The adopted strategy is based on generating virtual ground control points using rational polynomials intersection by means of available RPCs. The generated virtual GCPs provide a reliable data for estimating the degree of fitness of the 3D affine model to the rational polynomial transformation. This paper reports the result of the tests conducted on a high resolution stereo IRS-P5 satellite image. Other related issues including different methods for estimating initial values needed for the solution of the rational polynomials intersection, such as DLT, 3D affine and truncated rational polynomials are also presented and discussed.

### 1. INTRODUCTION

After the recent Tsunami and earthquake disasters with their devastating effects, the information content of the linear array satellite imageries as a means for the disaster forecasting and management has gained much more importance than before. One of the crucial preliminary stages after any natural disaster is the rapid mapping of the damaged areas using satellite imageries. This process entails a great deal of computations and field works which hinder the rapid response to the preliminary mapping demands. Two main approaches are used for geo-coding of linear array imageries. The first approach is the so called rigorous model. This approach is based on the physical modeling of the linear array motion and attitude variations. However, this Method may not be appropriate for rapid mapping since it requires necessary orbital information as well as the sensor calibration parameters which may not be accessible. The second approach uses the rational polynomial model (RFM) as a replacement for the rigorous method. Again, the RFM coefficients are included in the metadata and may not be accessible in all circumstances. The solution of the RFM also requires the regularization and normalization. The RFM intersection is solved iteratively and hence demanding initial values for the object coordinates. Moreover, the solution may undergo computational collapse for a given dataset. These complications make these approaches non-optimal for rapid mapping applications. Taking into account the fact that high resolution satellite images inevitably have large focal length, it can be seen immediately that these imageries enjoy a very narrow field of view. The very small camera field of view makes the incoming signals almost parallel. This particular geometry provides a simple linear-parallel relationship between

the image space and the object space and makes a simple eight parameters affine transformation optimum for geo referencing applications. Simplicity of the formulation (i.e. only eight affine parameters for the entire scene), few numbers of required GCP's and the achieved accuracy makes this approach very attractive from the rapid mapping point of view. Nevertheless, in practice several unpredicted factors may influence the accuracy of the transformation. One of the major influential factors in this respect is the terrain relief undulations. This approach has been already evaluated by different researchers worldwide and reasonably accurate results have been reported using only few numbers of GCP's (Fraser et al., 2004; Fraser et al., 2003; Yamakawa et al 2004). The main task undertaken in this study is to investigate the fitness accuracy of the 3D affine model with the RFM, as far as the terrain independent scenario is concerned. The adopted strategy for the evaluation of the preliminary results is based on the generation of a network of the so called virtual GCP's whose coordinates are obtained by the available RPC's. Few number of well distributed virtual GCP's serve as the reference data to determine the transformation parameters of the 3D affine transformation and the rest of the virtual ground points are considered as check points for the evaluation of the absolute accuracy. All accuracy figures are presented for the check points in the object space. This strategy for the accuracy evaluation adopts the accuracy of the virtual ground points generated by the RPCs as a criterion for the evaluation of the fitness accuracy of the affine model.

In the sections that follow the basic concepts of the RFM and the 3D affine models are reviewed first. This is then followed by the review of the formulations of the RFM intersection. The

last section deals with the evaluation of the fitness accuracy obtained on the stereo IRS-P5 images acquired over a test site.

**1.1 Rational Function Model**

The concept of RFM was developed by Gyer (Sadeghian, 2001). This model project the 3D object space coordinate into a 2D image coordinate and could be used for any type of images; airborne or space borne. The Rational Function Model is expressed as a ratio of two polynomials:

$$x = \frac{F_1^r(X, Y, Z)}{F_2^r(X, Y, Z)} \tag{1}$$

$$y = \frac{F_3^r(X, Y, Z)}{F_4^r(X, Y, Z)}$$

Where:  $x, y$  = are the normalized image coordinates  
 $X, Y, Z$  = are the normalized object coordinates  
 $F_i^r$  is the  $r$  order polynomials

$r$  is the order of polynomials which is usually equal to 3 so the rational model would be the ratio of two cubic polynomials and each polynomial has 20 terms making a total of 80 parameters which is reduced to 78: i.e.

$$x = \frac{(1ZX Y ..Y^3 X^3) \cdot (a_0 a_1 .. a_{19})^T}{(1ZX Y ..Y^3 X^3) \cdot (b_0 b_1 .. b_{19})} \tag{2}$$

$$y = \frac{(1ZX Y ..Y^3 X^3) \cdot (c_0 c_1 .. c_{19})}{(1ZX Y ..Y^3 X^3) \cdot (d_0 d_1 .. d_{19})}$$

In order to increase the stability of equation, it is essential to normalize the two image coordinates and three object coordinates using shift and scale parameters to fit the range -1 ~ +1. The normalizing equation can be described as:

$$x' = \frac{x - x_0}{x_s}, \quad y' = \frac{y - y_0}{y_s} \tag{3}$$

$$X' = \frac{X - X_0}{X_s}, \quad Y' = \frac{Y - Y_0}{Y_s}, \quad Z' = \frac{Z - Z_0}{Z_s}$$

Where:  $x_0, y_0$  = are shift values for image coordinate  
 $x_s, y_s$  = are the scale value for image coordinate  
 $X_0, Y_0, Z_0$  = are shift value for object coordinate  
 $X_s, Y_s, Z_s$  = are the scale value for object coordinate

The unknown parameters involved in RFM can be determined with or without using the rigorous sensor model. Therefore two computational scenarios are present, terrain dependent and terrain independent (Grodecki et al., 2004).

**1.1.1 Terrain dependent scenario:** When there is no rigorous sensor model at hand, one has to measure control points and check points from both images and the actual DEM or maps. In this case, the solution is heavily dependent on the actual terrain relief, number of control points and distribution of control points (Tao C V, Hu Y, 2001).

**1.1.2 Terrain independent scenario:** When the rigorous sensor model is available, the RFCs can be determined via 3D object grid with corresponding image points which are determined through rigorous model. In this case, the solution is actually terrain independent since no terrain information is used (Tao C V, Hu Y, 2001). The method has three main steps:

First, determination of a grid of sufficient image points,  
 Second, set up a 3D grid of object points via rigorous model, in this step, rigorous parameters -which are measured using onboard GPS receivers and gyros-are used to compute the corresponding object coordinates of image points.  
 Third, RFM fitting, the RPCs are computed using image coordinates and their corresponding object coordinates by applying space resection.

**1.1.3 The Bias Compensated RPC:** Exterior orientation parameters which comprise position and attitude are used to calculate RPCs in terrain independent mode. On-board GPS receivers determine the satellite ephemeris. Star tracker and gyros determine attitude as a function of time. Ephemeris and attitude have finite accuracy, about one meter for ephemeris and one or two arc-second for attitude [8]. As a result, the calculated RPCs in terrain independent mode have bias. Many research works have already been conducted as regards the methods and the accuracy of the bias removal. It has been demonstrated that the bias can be compensated via one shift parameter in line direction and one shift parameter in sample direction (Dial & Grodecki 2002).

$$x + A_0 = \frac{F_1^r(X, Y, Z)}{F_2^r(X, Y, Z)} \tag{4}$$

$$y + B_0 = \frac{F_3^r(X, Y, Z)}{F_4^r(X, Y, Z)}$$

The bias compensated RPCs can be computed as:

$$F_1(X, Y, Z) = (a_1 - b_1 A_0) + (a_2 - b_2 A_0) \cdot X$$

$$+ \dots + (a_{20} - b_{20} A_0) \cdot Z^3 \tag{5}$$

$$F_3(X, Y, Z) = (c_1 - d_1 B_0) + (c_2 - d_2 B_0) \cdot X$$

$$+ \dots + (c_{20} - d_{20} B_0) \cdot Z^3$$

The accuracy of this model has been reported less than 0.5 pixels (Hanley & Fraser, 2004). Parameters for drift can also be added.

**1.2 3D Affine Transformation**

Affine model is a linear transformation which maps the 3D object space into 2D image space through 8 parameters, as shown in equation (5):

$$x = A_1 X + A_2 Y + A_3 Z + A_4 \tag{5}$$

$$y = A_5 X + A_6 Y + A_7 Z + A_8$$

Where  $A_{1, \dots, 8}$  = affine parameters

Equation 5 accounts for two translations, three rotations and non uniform scaling and skew distortions within image space. It could be regarded as a first order rational function with the denominator equal to one.

Strictly speaking, the imaging geometry of a satellite push broom scanner can be described as perspective in the line of the linear array and parallel in the along-track direction. However, with a very narrow field of view, the assumption that the projection is parallel stands true in practical cases (Fraser & Yamakawa, 2004).

**1.3 DLT Model**

Direct linear transformation, which is a first order rational function, maps 3D object space into 2D image space via 11 parameters:

$$\begin{aligned}
 x &= \frac{L_1 X + L_2 Y + L_3 Z + L_4}{L_5 X + L_6 Y + L_7 Z + 1} \\
 y &= \frac{L_8 X + L_9 Y + L_{10} Z + L_{11}}{L_5 X + L_6 Y + L_7 Z + 1}
 \end{aligned}
 \tag{6}$$

Where  $L_1, \dots, L_{11}$  = DLT parameters

DLT parameters can be computed directly using EOP and IOP parameters or indirectly using GCPs. This model is considered as an approximate model for linear array scanner since the EOP parameters are not the same for all image lines (Morgan, 2004).

**2. VIRTUAL GCP GENERATION**

As explained before, fitness accuracy of the 3D affine model as compared with the RFM model is evaluated by generating virtual GCPs. These points are calculated via the RPCs accessible in the IRS-P5 metadata. This is explained in the section that follows.

**2.1 RFM Intersection**

The rational function model which is presented as equation (1) is always referred to as forward RPC model which provides a mapping from geographic coordinate of object  $(\varphi, \lambda, h)$  to image coordinate  $(s, L)$ . Denormalizing equation (1) yields:

$$\begin{aligned}
 x &= r(\varphi, \lambda, h), y = p(\varphi, \lambda, h) \\
 x &= \frac{F_1^3(X, Y, Z)}{F_2^3(X, Y, Z)} x_s - x_0 \\
 y &= \frac{F_3^3(X, Y, Z)}{F_4^3(X, Y, Z)} y_s - y_0
 \end{aligned}
 \tag{7}$$

$$\text{Where } X = \frac{\lambda - \lambda_0}{\lambda_s}, Y = \frac{\varphi - \varphi_0}{\varphi_s}, Z = \frac{h - h_0}{h_s}$$

Because of nonlinearity of the equation, applying the Taylor series expansion gives (Grodecki et al., 2004).

$$\begin{aligned}
 x &= r(\varphi_0, \lambda_0, h_0) + \left. \frac{\partial r}{\partial w^T} \right|_{z=z_0} dw \\
 y &= p(\varphi_0, \lambda_0, h_0) + \left. \frac{\partial p}{\partial w^T} \right|_{z=z_0} dw
 \end{aligned}
 \tag{8}$$

The derivation can be calculated through some partial derivations as follow (Grodecki et al., 2004):

$$\begin{aligned}
 \frac{\partial r}{\partial w^T} &= \frac{\partial r}{\partial u^T} \frac{\partial u}{\partial v^T} \frac{\partial v}{\partial w^T} \\
 \frac{\partial p}{\partial w^T} &= \frac{\partial p}{\partial u^T} \frac{\partial u}{\partial v^T} \frac{\partial v}{\partial w^T}
 \end{aligned}
 \tag{9}$$

Where:

$$\begin{aligned}
 u &= [1, X, Y, Z, XY, XZ, YZ, X^2, Y^2, Z^2, XYZ, \\
 &X^3, XY^2, XZ^2, X^2Y, Y^3, YZ^2, X^2Z, Y^2Z, Z^3] \\
 v &= [X \quad Y \quad Z], w = [\lambda, \varphi, h]
 \end{aligned}$$

To evaluate the object space coordinate of a point we should measure the image coordinate in at least a stereo image. In this solution we use two stereo forward and afterward images. The equation would read as follow (Grodecki et al., 2004).

$$\begin{aligned}
 x^F &= r^F(\varphi, \lambda, h) + \varepsilon_x^F \\
 y^F &= p^F(\varphi, \lambda, h) + \varepsilon_y^F \\
 x^A &= r^A(\varphi, \lambda, h) + \varepsilon_x^A \\
 y^A &= p^A(\varphi, \lambda, h) + \varepsilon_y^A
 \end{aligned}
 \tag{10}$$

The final observation equations follow with (Grodecki et al., 2004).

$$A dw = L \tag{11}$$

Where:

$$A = \begin{bmatrix} \frac{\partial r^F}{\partial w^T} \\ \frac{\partial p^F}{\partial w^T} \\ \frac{\partial r^A}{\partial w^T} \\ \frac{\partial p^A}{\partial w^T} \end{bmatrix}, dw = [d\lambda, d\varphi, dh]^T, L = \begin{bmatrix} x^F - r^F(\varphi_0, \lambda_0, h_0) \\ y^F - p^F(\varphi_0, \lambda_0, h_0) \\ x^A - r^A(\varphi_0, \lambda_0, h_0) \\ y^A - p^A(\varphi_0, \lambda_0, h_0) \end{bmatrix}$$

The unknown object space coordinate is solved for iteratively. At the first iteration, the initial value for coordinates is needed which could be determined through linear equations such as 3D affine or DLT. Alternatively, truncated RPCs can also be used. At each iteration step, application of least squares, results in correction of approximate values of object coordinates, i.e.:

$$dw = (A^T A)^{-1} A^T L \tag{12}$$

$$w_0^i = w_0^{i-1} + dw \tag{13}$$

### 2.2 Affine Intersection

For evaluating the object space coordinate using affine transformation, one should calculate its 8 parameters of each image at first by applying at least four GCPs:

$$\begin{bmatrix} X, Y, Z, 0, 0, 0 \\ 0, 0, 0, X, Y, Z \end{bmatrix} [A_1, \dots, A_8]^T = \begin{bmatrix} x \\ y \end{bmatrix} \tag{14}$$

After evaluation of the parameters, by measuring image coordinate of any point in a stereo image, its object coordinates could be determined via the following relations:

$$\begin{bmatrix} A_1^F, A_2^F, A_3^F \\ A_5^F, A_6^F, A_7^F \\ A_1^A, A_2^A, A_3^A \\ A_5^A, A_6^A, A_7^A \end{bmatrix} \cdot \begin{pmatrix} X \\ Y \\ Z \end{pmatrix} = \begin{pmatrix} x^F - A_4^F \\ y^F - A_8^F \\ x^A - A_4^A \\ y^A - A_8^A \end{pmatrix} \tag{15}$$

Iterative least squares solution of Equation 10 yields the object coordinates for the virtual GCPs. This step is then followed by the solution of Equation 14 through which 3D affine parameters are derived using any combination of the well distributed virtual GCPs. Subsequently, for any virtual GCP whose scan and line coordinates is already measured, new object coordinates can be determined via Equation 15. The final fitting accuracy evaluation is then performed by comparing the object coordinates of the GCPs calculated by Equation 10 and the object coordinates computed by Equation 15. Next section presents the result of the tests conducted on IRS-P5 stereo image.

## 3. EXPERIMENTAL RESULT

### 3.1 Data Set

A stereo orthokit image of the IRS-P5 satellite imagery over the city of Arak, Iran which were acquired in 2007, are used in the test. The RPC parameters were available for both forward and afterward images. Figure 1 shows parts of the stereo dataset used in the project.

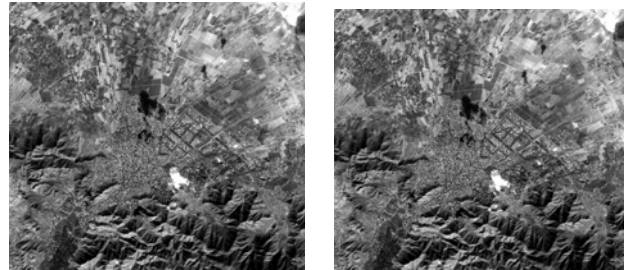


Figure1. Afterward (left) and forward (right) images of stereo dataset.

As mentioned before, for the solution of Equation 10 approximate object coordinates are required. The image coordinates of 18 virtual GCPs are measured. Three methods are implemented to generate the approximate coordinates, namely: 3D affine, DLT and truncated RPCs. The achieved results for RPC intersection by applying different method for evaluating the initial values have been presented in Table1.

Method	ΔE(m)	ΔN(m)	Δh(m)	Iteration
3D affine	2.42	3.11	6.40	11
DLT	2.42	3.11	6.40	14
Truncated RPC	2.42	3.11	6.40	15

Table2. Results of RPC intersection, applying different methods for evaluating initial value.

As the Table 1 indicates, all methods of deriving approximate values have produced reasonably accurate initial values and the equations have been successfully converged. It is interesting to note that the affine model for calculating approximate values has lead to smaller number of iterations in the solution of Equation 10. This implies that the affine model generates more accurate results as compared to the other two approaches.

Distribution of the generated virtual GCPs is presented in Figure 2.

Having determined the object coordinates of the virtual GCPs, in the next step the 3D affined parameters (Equation14) are solved to derive the 8 affine parameters by applying different number of GCPs and CPs. This is followed by the solution of Equation 15 to derive the object coordinates of all virtual GCPs. The residual vectors for the height and planimetric coordinates when 5 GCPs were used are presented in Figures 3 and 4 respectively.

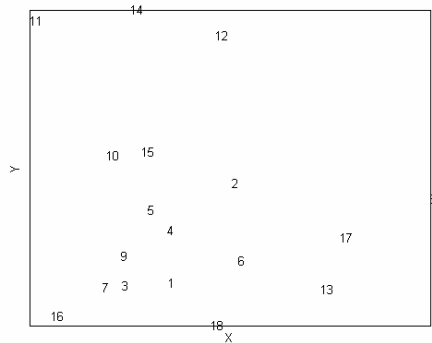


Figure 2. Distribution of generated virtual GCPs

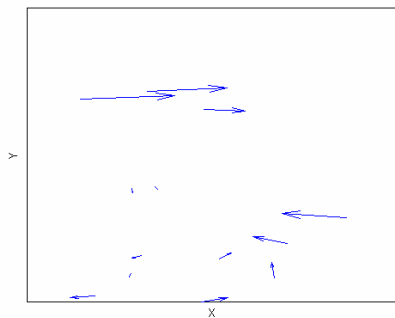


Figure 3. the residual vectors of planimetric coordinates.

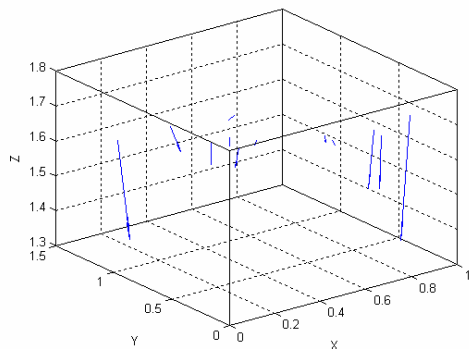


Figure 4. the residual vectors of 3D object coordinates.

As the Figure 3 indicates and according to Table 3, the X and Y residuals are quite small implying accurate planimetric fitting potential of the 3D affine model. However, the height residuals do not indicate high fitting accuracy. This shows that as far as the height values are concerned, there is a non-linearity in the image data that the linear terms of the 3D affine cannot take it into account. However, another reason for the lower height fitting accuracy may be the measurement errors during the homologous points identification and measurement stage.

### CONCLUDING REMARKS

The overall results achieved in this study further supports the conclusions arrived by other researchers as regards the applicability of the 3D affine transformation as a replacement model for the more sophisticated RFM. This statement is true under the proviso that the strip length does not exceed the size of a high resolution satellite frame.

### REFERENCES

- Dial, Gene and Jacek Grodecki 2002. Block Adjustment with Rational Polynomial Camera Models. Proceedings of ASPRS 2002 Conference, Washington, DC, April 22-26, 2002.
- Fraser, C.S., and T. Yamakawa, 2003, Applicability of the Affine Model for IKONOS Image Orientation over Mountainous Terrain. In Proc. of ISPRS-EARSeL Joint Work on "High Resolution Mapping from Space", Hannover, on CDROM.
- Fraser, C.S. & T. Yamakawa, 2004. Insights into the affine model for satellite sensor orientation. ISPRS Journal of Photogrammetry and Remote Sensing, 275-288
- Grodecki, J., Dial, G., Lutes, J., 2004. Mathematical Models For 3D Feature Extraction From Multiple Satellite Images Described By RPCs. ASPRS Annual Conference Proceeding, May 2004.
- Hanley, H.B. and Fraser, C.S., 2004. Sensor Orientation for High-Resolution Satellite Imagery: Further Insights into Bias-Compensated RPCs. *International Archives of the Photogrammetry, Remote Sensing and Spatial Information Sciences*, 35(B1): 24-29.
- Morgan, M., 2004, Epipolar Resampling of Linear Array Scanner Scenes, PhD Dissertation, Department of Geomatics Engineering, University of Calgary, Canada.
- Okamoto, A., Fraser, C., Hattori, S., Hasegawa, H., Ono, T., 1998. An alternative approach to the triangulation of SPOT imagery. *International Archives of Photogrammetry and Remote Sensing* 32 (B4), 457- 462.
- Yamakawa T., Fraser C.S., 2004, The affine projection model for sensor orientation: experiences with high-resolution satellite imagery, IAPRS of 20th Congress, Commission I, WG V/5, Istanbul (CD).
- Tao C V, Hu Y, 2001. The Rational Function Model: a tool for processing high-resolution imagery. *Earth Observation Magazine*, 10(1):13-16.
- Savopol, F., Armenakis, C., 1998. Modelling of the IRS-1C satellite pan imagery using the DLT approach. *International Archives of Photogrammetry and Remote Sensing*, Vol. 32, Part 4, pp. 511-514.
- Sadeghian, S., M. J. Valadan Zoej, M. R. Delavar, A. Abootalebi, 2001. Precision Rectification of High Resolution Satellite Imagery Without Ephemeris Data, *International Journal of Applied Earth Observation and Geoinformation (JAG)*, 3 (4): 366-371.
- Wang, Y., 1999. Automated Triangulation of Linear Scanner Imagery, Joint Workshop of ISPRS WG I/1, I/3 and IV/4, Sensors and Mapping from Space, Hanover, September, 27-30.

No. GCPs(CPs)								
4(14)			5(13)			6(12)		
$\Delta X(m)$	$\Delta Y(m)$	$\Delta Z(m)$	$\Delta X(m)$	$\Delta Y(m)$	$\Delta Z(m)$	$\Delta X(m)$	$\Delta Y(m)$	$\Delta Z(m)$
0.068	0.1238	0.336	0.1013	0.0634	-0.305	-0.004	0.0328	0.114
0.058	0.0281	-0.221	0.0161	0.0363	-0.006	-0.751	-0.089	-4.484
0.008	0.0412	0.093	-0.551	0.0398	-5.061	-0.09	-0.071	-0.409
-0.706	-0.163	-5.279	-0.084	-0.027	-0.148	0.1544	0.0901	-1.056
-0.095	-0.099	-0.568	0.0097	-0.041	-0.898	1.129	0.3264	-4.642
0.199	0.296	-0.005	0.8014	0.0366	-4.231	0.4483	0.0897	0.1681
1.201	0.7388	-2.422	0.3517	-0.017	0.142	-0.144	0.1146	-1.644
0.513	0.298	1.093	-0.018	0.1646	-2.223	0.8764	0.2183	-1.373
-0.1	0.1073	-1.987	0.675	0.0395	-1.124	0.1159	0.0505	-0.518
0.941	0.5079	0.091	0.0204	-0.027	-0.351	-0.175	0.0506	-0.536
0.152	0.1952	0.184	-0.214	-0.02	-0.735	-0.424	-0.009	-2.057
-0.152	0.1383	-0.108	-0.295	0.0808	-2.379	0.0951	-0.121	-0.398
-0.391	-0.052	-2.565	0.2274	0.0404	-0.259			
0.074	-0.288	-1.37						

Table3. Results of affine intersection.

No.GCPs(CPs)	$\Delta X(m)$	$\Delta Y(m)$	$\Delta Z(m)$
4(14)	0.51	0.3	1.92
5(13)	0.38	0.063	2.18
6(12)	0.53	0.14	2.18

Table4. Total RMSE for affine intersection.